CDDpress

www.nature.com/cdd

ARTICLE

Check for updates

PHGDH/SYK: a hub integrating anti-fungal immunity and serine metabolism

Xinyong Zhang[1,9], Dongdong Hu[2,9], Xiaoyan Sun[3,9], Yichun Gu[4], Yong Zhou[1], Chuanxin Su[5], Shi Liu[6], Caiyan Zhang[7], Guoping Lu[7], Qiwen Wu[8]✉ and Aidong Chen[4]✉

Immune cells modify their metabolic pathways in response to fungal infections. Nevertheless, the biochemical underpinnings need to be better understood. This study reports that fungal infection drives a switch from glycolysis to the serine synthesis pathway (SSP) and one-carbon metabolism by inducing the interaction of spleen tyrosine kinase (SYK) and phosphoglycerate dehydrogenase (PHGDH). As a result, PHGDH promotes SYK phosphorylation, leading to the recruitment of SYK to C-type lectin receptors (CLRs). The CLR/SYK complex initiates signaling cascades that lead to transcription factor activation and pro-inflammatory cytokine production. SYK activates SSP and one-carbon metabolism by inducing PHGDH activity. Then, one-carbon metabolism supports S-adenosylmethionine and histone H3 lysine 36 trimethylation to drive the production of pro-inflammatory cytokines and chemokines. These findings reveal the crosstalk between amino acid metabolism, epigenetic modification, and CLR signaling during fungal infection.

Cell Death & Differentiation; https://doi.org/10.1038/s41418-024-01374-7

INTRODUCTION

Human health is severely threatened by fungal infections, particularly in immunocompromised individuals, such as those who have human immunodeficiency virus infections, primary immunological deficiencies, are undergoing chemotherapy, or have received an organ transplant [1, 2]. The two most common opportunistic fungal infections that affect people are *Candida albicans* and *Aspergillus fumigatus* (*Af*) [3, 4]. Although several anti-fungal medications work well, drug resistance is quickly developing, which is becoming an increasing concern [5]. Both *Af* infections and *C. albicans* have death rates higher than 30% [5]. Toll-like receptors (TLRs) and CLRs are two examples of pattern recognition receptors that host cells utilize to identify pathogen-associated molecular patterns from fungi during fungal infection [6]. Dectins-1, -2, -3, and mincle are among the CLRs identifying β-glucan, α-mannan, and fungal glycolipids in that order [7]. Protein kinase C-δ (PKC-δ) is activated through CLR agonist ligation and spleen tyrosine kinase (SYK) recruitment that follows [8]. The development of domain-containing protein 9 (CARD9), B cell lymphoma/leukemia 10 (BCL10), and mucosa-associated lymphoid tissue 1 (MALT1) is facilitated by signaling via PKC-δ [9]. Subsequently, pro-inflammatory cytokines and chemokines are produced when the CARD9/BCL10/MALT1 complex activates mitogen-activated protein kinase with NF-κB and NFAT transcription factors [10]. By dephosphorylating SYK, tyrosine phosphatase SHP-1 adversely regulates SYK activity [11].

It was discovered sixty years ago that children with acute lymphoblastic leukemia could experience remission while using the folate antagonist aminopterin [12]. Since then, there has been substantial investigation into the significance of one-carbon metabolism in cancer. Cells can produce one-carbon units through one-carbon metabolism, which depends on the folate and methionine cycles and is necessary for producing lipids, amino acids, and S-adenosylmethionine (SAM) [13, 14]. The latter is the primary source of methyl for cellular methylation reactions [15]. Several processes, such as the metabolism of choline, serine, and other amino acids to glycine, produce one-carbon units [16]. One non-essential amino acid that can be produced de novo from glucose is serine [17]. Three different metabolic routes process glucose when it is internalized through GLUT: glycolysis, the serine synthesis pathway (SSP), and the pentose phosphate pathway (PPP) [18]. At the first committed stage of glucose metabolism, the PPP diverges from glycolysis to produce ribonucleotides [19]. The PPP also maintains cellular redox homeostasis by reducing glutathione (GSH) by producing nicotinamide adenine dinucleotide phosphate (NADPH) [20]. Phosphoglycerate dehydrogenase (PHGDH), phosphoserine aminotransferase 1 (PSAT1), and phosphoserine phosphatase (PSPH) are the three metabolic enzymes that drive the synthesis of serine from 3-phosphoglycerate (3PG) [21]. Next, the methyltransferases SHMT1 and SHMT2 convert serine to glycine, which causes the one-carbon unit to be cleaved

[1]Department of Neurology, The Second People's Hospital of Huai 'an, Huai 'an 223001, China. [2]Department of Emergency, The Fourth Affiliated Hospital of Nanjing Medical University, Nanjing 210031, China. [3]School of Food and Pharmacy, Zhejiang Ocean University, Zhoushan 316022, China. [4]The Key Laboratory of Targeted Intervention of Cardiovascular Disease, Collaborative Innovation Center for Cardiovascular Disease Translational Medicine, and Department of Physiology, Nanjing Medical University, Nanjing, Jiangsu 211166, China. [5]The Key Laboratory of Targeted Intervention of Clinical Disease, University Hospital Essen, University of Duisburg-Essen, Essen 45122, Germany. [6]State Key Laboratory of Virology, Modern Virology Research Center, Frontier Science Center for Immunology and Metabolism, College of Life Sciences, Wuhan University, Wuhan 430072, China. [7]Department of Critical Care Medicine, Children's Hospital of Fudan University, Shanghai, China. [8]Department of Laboratory Medicine, The First Affiliated Hospital of Wannan Medical College, Wuhu 241001, China. [9]These authors contributed equally: Xinyong Zhang, Dongdong Hu, Xiaoyan Sun ✉email: yjslab@163.com; aidongchen@njmu.edu.cn

Received: 10 October 2023 Revised: 29 August 2024 Accepted: 2 September 2024
Published online: 10 September 2024

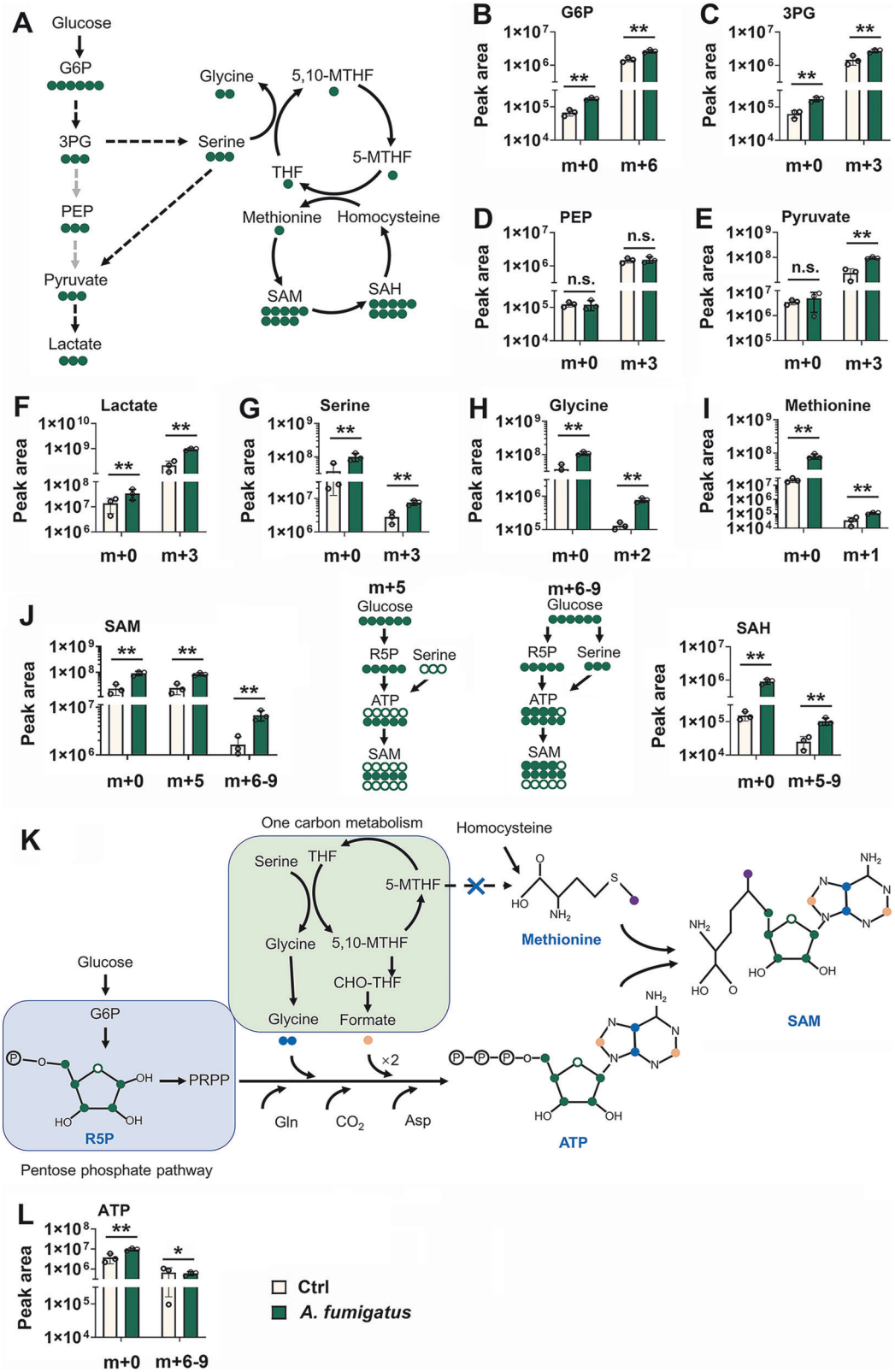

Fig. 1 Fungal infections drive glucose flux from glycolysis to the SSP and one-carbon metabolism. A Schematic of ^{13}C-glucose carbon labeling through glycolysis, the SSP, folate cycle, the methionine cycle, and SAM generation. BMDMs were infected with or without *Af* for 6 h. ^{13}C-glucose incorporation into G6P **B**, 3PG **C**, PEP **D**, pyruvate **E**, lactate **F**, serine **G**, glycine **H**, methionine **I**, SAM and SAH **J** were analyzed ($n = 3$ mice per condition, two-way ANOVA, mean ± SEM). **K** Schematic of derivation and contribution of carbon atoms in SAM synthesis (green, carbon atoms resourced from the PPP; blue, carbon atoms from glycine; yellow, carbon atoms from one-carbon metabolism; CHO-THF, 10-formyl tetrahydrofolate). **L** BMDMs were infected with or without *Af* for 6 h. ^{13}C-glucose incorporation into and ATP were analyzed ($n = 3$ mice per condition, two-way ANOVA, mean ± SEM). (**$P < 0.01$, *$P < 0.05$, n.s., not significant). See also Fig. S1.

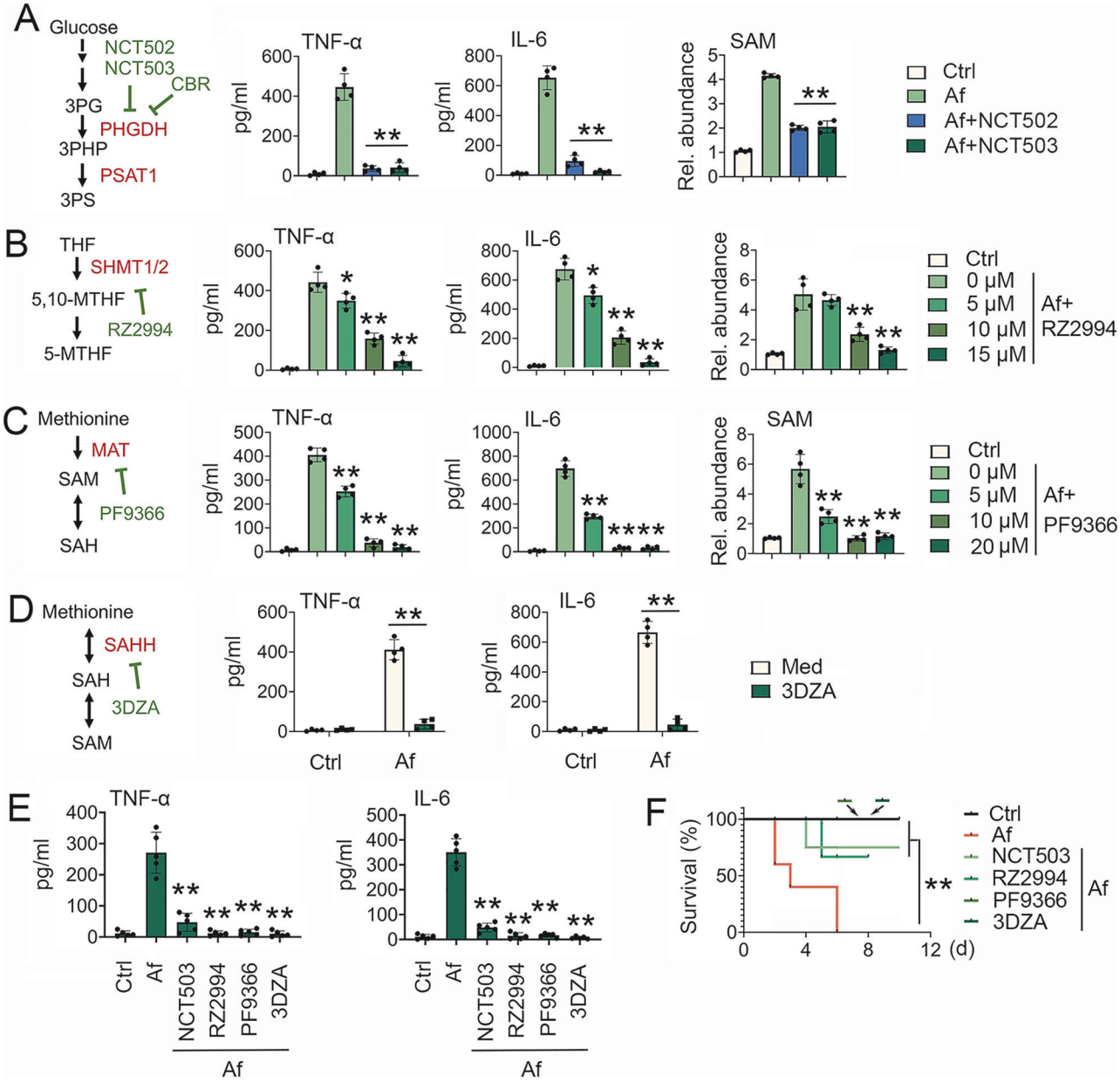

Fig. 2 The SSP, one-carbon metabolism, and SAM are required for anti-fungal innate immunity. A BMDMs were infected with or without *Af* and treated with or without PHGDH inhibitors (50 mM) for 6 h. Levels of pro-inflammatory cytokines were measured using ELISA. **B** BMDMs were infected with or without *Af* and treated with or without the indicated concentration of RZ2994. Levels of TNF-α and IL-6 were measured using ELISA, and levels of SAM were measured using LC-MS. **C** Experiments were performed as described in (B), except the indicated concentration of PF9366 was used. **D** Experiments were performed as described in **A**, except 3DZA (1 μM) was used. **E** C57BL/6 mice were infected with or without *Af* and treated with or without NCT503 (50 mg/kg), RZ2944 (30 mg/kg), PF9366 (15 mg/kg) or 3DZA (10 mg/kg) for 24 h. Levels of TNF-α and IL-6 in the lung were measured using ELISAs. **F** Experiments were performed as described in **E**. Survival curves show Values collected until day ten after infection. Statistical analysis was performed using the log-rank test (n = 5 for each group). Values in **A–E** are presented as means ± SEMs, $n = 4$ per condition, two-way ANOVA. (**$P < 0.01$). See also Fig. S2.

from serine and transferred to tetrahydrofolate (THF) [22]. Formyl-THF, methyl-THF, and methylene-THF are produced by THF accepting one carbon unit [23]. These compounds provide one carbon unit for purine synthesis, the methionine recycling pathway, and thymidylate synthesis [23]. Methylenetetrahydrofolate dehydrogenase, or MTHFD, facilitates the conversion of methylene-THF to formyl-THF during anabolism, which is necessary for purine biosynthesis [24].

The Warburg shift and glutamine metabolism are necessary for anti-fungal immune responses [25]. One-carbon units, however, have not yet been demonstrated to act as immunomodulators of innate immunity against fungi. In this study, we observed the synergistic effects of PPP, SSP, and one-carbon metabolism on anti-fungal innate immunity by modulating the availability of SAM to support the epigenetic reprogramming of histone methylation. SYK associates with PHGDH during fungal infection, shifting glucose metabolism from glycolysis to SSP and one-carbon metabolism. These results imply that during fungal infection, there is a direct connection between the "immune state," the "metabolic state," and the "chromatin state."

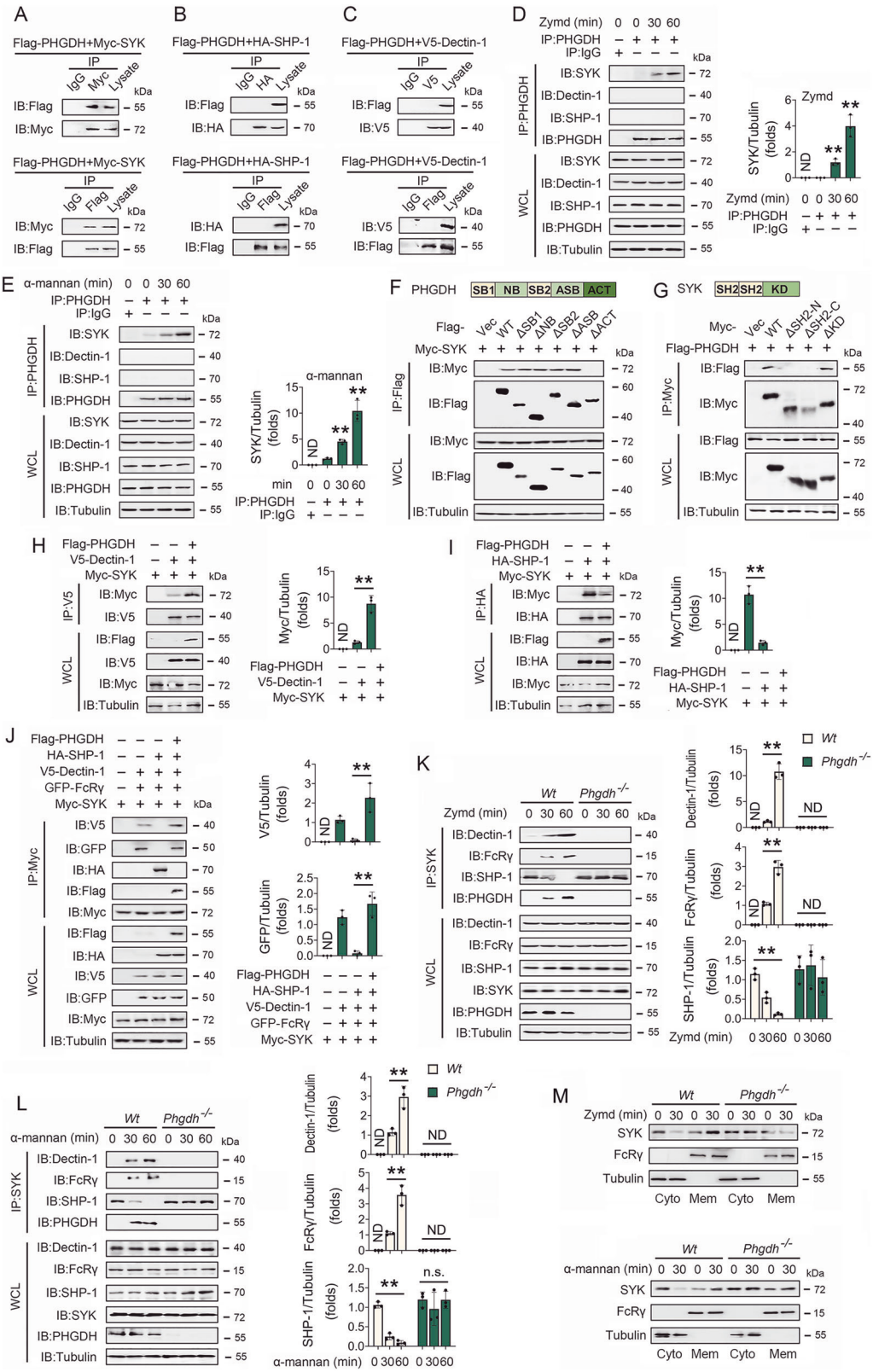

RESULTS

Fungal infection shifts energy metabolism to PPP, SSP, and one-carbon metabolism

To ascertain the impact of fungal infection on glucose metabolism reprogramming, we conducted measurements of ^{13}C-glucose incorporation through glycolysis, the PPP, the SSP, and one-carbon metabolism (Fig. 1A). *Af*-infected bone marrow-derived macrophages (BMDMs) displayed higher ^{13}C-glucose incorporation into glucose-6-phosphate (G6P), 3PG, pyruvate, lactate, serine, glycine, and methionine; however, not phosphoenolpyruvate (PEP) (Fig. 1B–I), indicates increased glycolytic flow to the SSP and one-carbon metabolism. Notably, *Af*-infected

Fig. 3 SYK associates with PHGDH. A–C HEK293 cells were transfected with indicated plasmids for 48 h. Co-IP and immunoblot analyses were performed using the indicated antibodies. **D, E** BMDMs were stimulated with zymd (100 μg/ml) **D** and α-mannan (100 μg/ml) **E** for the indicated times. Co-IP and immunoblot analyses were performed using the indicated antibodies. Quantification of the immunoblots is shown on the right panel. **F** Schematic diagram of the full-length and truncated constructs of PHGDH (upper panel). HEK293 cells were co-transfected with Myc-SYK and the indicated truncated PHGDH constructs for 48 h. Co-IP and immunoblot analyses were performed with the indicated antibodies (lower panel). **G** Experiments were performed similarly to those in **F**, except the indicated truncated constructs of SYK were used. **H–J** HEK293 cells were transfected with indicated plasmids for 48 h. Co-IP and immunoblot analyses were performed using the indicated antibodies. Quantification of the immunoblots is shown on the right panel. (K and L) *Phgdh* $^{+/+}$ (*Wt*) and *Phgdh* $^{-/-}$ BMDMs were stimulated with zymd (100 μg/ml) **K** and α-mannan (100 μg/ml) **L** for the indicated time. Co-IP and immunoblot analyses were performed using the indicated antibodies. Quantification of the immunoblots is shown on the right panel. **M** *Wt* and *Phgdh* $^{-/-}$ BMDMs were stimulated with zymd (100 μg/ml) and α-mannan (100 μg/ml) for the indicated times, and whole-cell lysates were separated into membrane and cytosolic fractions-immunoblot analysis with antibodies. All experiments were repeated at least three times. Values are presented as means ± SEMs, two-way ANOVA. (**$P < 0.01$, ND, not detective) See also Fig. S3.

BMDMs had low labeling of m + 1 methionine and high unlabeled m + 0 methionine, suggesting that uptake of exogenous methionine expanded the intracellular methionine pool (Fig. 1I). Glucose-derived SAM synthesis and the result of SAM demethylation (S-adenosylhomocysteine, or SAH) via two different pathways: one provides materials needed for de novo ATP synthesis, including the two carbons that glycine donates and the two one-carbon units that the THF cycle produces. The other function as methyl donors to facilitate homocysteine's re-methylation. (Figs. 1J and 1K). In this vein, *Af* infection increased the m + 5 labeled SAM (via the PPP), and m + 6–9 (via both the PPP and SSP) labeled SAM and SAH, suggesting that the methionine cycle is unlikely to be supported by glucose-derived one-carbon units (Fig. 1J). Further study revealed that *Af* infection mildly increased the m + 6–9 labeled ATP, suggesting that PPP, glycine, and THF cycle are involved in synthesizing glucose-derived SAM (Fig. 1K and 1L).

Since most of the *Af*-induced intracellular rise in serine was unlabeled (Fig. 1G and 1H), we speculate that additional mechanisms for serine entrance into one-carbon metabolism may exist. As shown in Fig. S1A, extracellular serine (m + 3) and glycine (m + 2) uptake were increased during *Af* infection. *Af* infection-derived ^{13}C-serine was incorporated into ADP, ATP, SAM, and SAH (Fig. S1B). As anticipated, exogenous ^{13}C-serine did not contribute to the methionine cycle (Fig. S1C). Next, we investigated whether *Af* infection would regulate inflammatory factors expression levels and essential markers of the SSP, PPP, and redox homeostasis. Accordingly, *Af* infection induced TNF-α and IL-6 protein levels in a time-dependent manner (Fig. S1D). Consistently, *Af* infection induced the activity of PHGDH and levels of serine, glycine, GSH/glutathione disulfide (GSSG) ratio, and the NADPH/NADP$^+$ ratio in a time-dependent manner (Fig. S1E–G). Similar results were obtained in *C. albicans*-infected BMDMs (Fig. S1H–S1K). These findings suggest that fungal infection induced the glycolysis offshoots to the PPP, the SSP, and one-carbon metabolism, leading to SAM generation.

The PPP, the SSP, and one-carbon metabolism are critical for anti-fungal innate immunity

The first rate-limiting enzyme of the SSP is called PHGDH. Its selective inhibitors include NCT502, NCT503, and CBR5884 (CBR) [26](Fig. 2A). These pathways, which were primarily impacted by NCT503 and CBR treatment, were linked to the inflammatory response and host defense, according to RNA- sequencing and pathway analysis (Fig. S2A and S2B). Consistently, *Af*-stimulated TNF-α, IL-6, and SAM levels were decreased in BMDMs treated with NCT502, NCT503, and CBR (Figs. 2A and S2C). It was recently identified that RZ-2994 inhibits both Shmt1 and Shmt2 [27] (Fig. 2B). RZ-2994 also inhibited *Af*-induced TNF-α, IL-6, and SAM in a dose-dependent manner (Fig. 2B). SAM is generated from methionine via methionine adenosyltransferase (Mat2a) [26]; therefore, we inhibited Mat2a with the allosteric inhibitor PF9366 and found that it decreased *Af*-induced intracellular SAM, TNF-α, and IL-6 (Fig. 2C). Because SAH, 3-Deazaadenosine (3DZA) inhibit methyltransferases is an inhibitor that reduces SAM-dependent methylation processes and lowers the SAM/SAH ratio by blocking SAH hydrolase [28] (Fig. 2D). Consistently, 3DZA treatment depressed *Af*-induced TNF-α and IL-6 (Fig. 2D).

To further determine the role of PHGDH, SHMT2, MTHFD2, MAT, and SAHH in anti-fungal innate immunity signaling, we purchased two specific small interfering RNAs (siRNAs) for PHGDH, SHMT2, MTHFD2, MAT, and SAHH. We tested their efficiency (Fig. S2D and S2E). The #2 of all siRNAs was selected for subsequent experiments. PHGDH, SHMT2, MTHFD2, MAT, and SAHH knockdown suppressed *Af*-induced TNF-α and IL-6 (Fig. S2F–S2J). Consistent with these results in vitro, NCT503, RZ-2994, PF9366, and 3DZA decreased levels of TNF-α and IL-6 in *Af*-infected mice (Fig. 2E). Moreover, NCT503, RZ-2994, PF9366, and 3DZA significantly increased the survival of mice challenged with *Af* (Fig. 2F). These findings suggest that an activated one-carbon flux and a downstream SAM generation are required for anti-fungal innate immunity.

Fungal infection regulates the SSP and CLR signaling via the PHGDH/SYK complex

To analyze the role of SSP in anti-fungal innate immunity, particularly verified ligands for both TLR signaling and CLR signaling were used, including pam3CSK (TLR1/2), poly(I:C) (TLR3), LPS (TLR4), imiquimod (TLR7), R-848 (TLR7), CpG ODN (TLR9), zymd (dectin-1), and alphα-mannan (dectin-2/3). Results from ELISA experiments confirmed that NCT503 treatment inhibited signaling via zymd and α-mannan but not ligands for TLRs (Fig. S3A), suggesting the specificity of SSP in regulating CLR signaling. Further study demonstrated that NCT503, RZ-2994, PF9366, and 3DZA also inhibited zymd and α-mannan -induced TNF-α and IL-6 protein levels (Fig. S3B and S3C). We created two distinct small interfering RNAs (siRNAs) for SYK, CAR9, BCL10, JNK, and p65 to screen the hub between CLR signaling and the SSP and evaluate their effectiveness (Fig. S3D). For subsequent tests, the #2 siRNA was chosen out of all the siRNAs. SYK, CAR9, BCL10, JNK, and p65 knockdown suppressed PHGDH-induced TNF-α and IL-6 expression (Fig. S3E), suggesting that PHGDH regulates CLR signaling via SYK. PHGDH, SHMT2, and MTHFD2 knockdown suppressed SYK-induced TNF-α and IL-6 expression (Fig. S3F), suggesting that SYK regulates CLR signaling via PHGDH.

Because SYK is upstream of CLR signaling cascades and PHGDH is the first rate-limiting enzyme of SSP [29], we speculated that SYK would directly interact with PHGDH. The results of coimmunoprecipitation (Co-IP) and reverse Co-IP assays showed that Flag-tagged PHGDH specifically interacts with Myc-tagged SYK but not with HA-tagged SHP-1 or V5-tagged dectin-1 (Fig. 3A–C). According to endogenous Co-IP assays, PHGDH did not interact with SYK in unstimulated cells. Still, as early as 30 min, zymd and α-mannan stimulation increased the association of

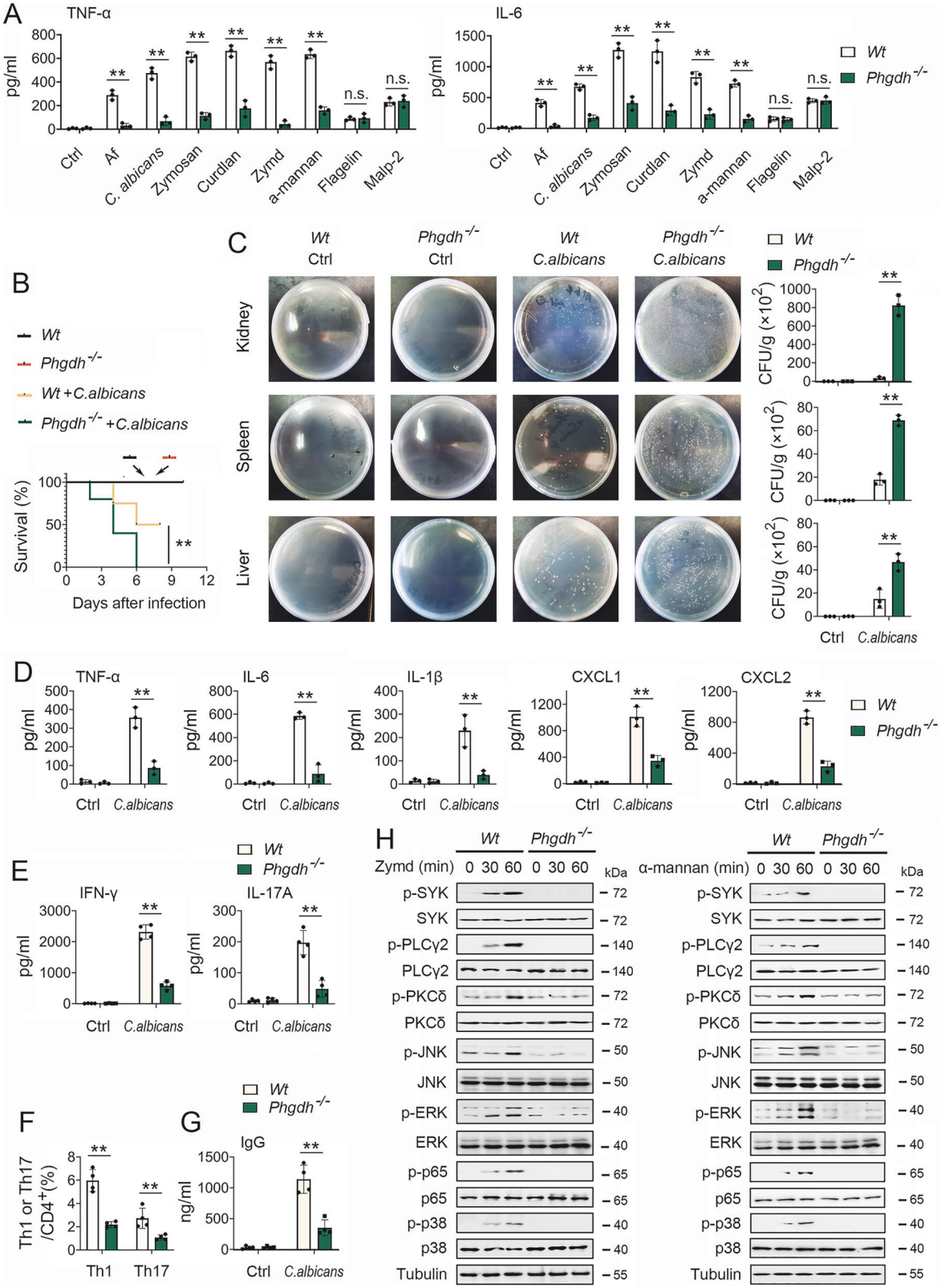

PHGDH and SYK (Fig. 3D and 3E). To conduct additional research on the PHGDH region that interacts with SYK, we generated PHGDH truncation mutants (Fig. 3F, upper panel). Co-IP experiments showed that the ACT domain of PHGDH was required for its interaction with SYK (Fig. 3F, lower panel). Similarly, the SH2 domain of SYK was required for its interaction with PHGDH (Fig. 3G). Next, we evaluated the impact of PHGDH on the association between SYK, dectin-1, and SHP-1. Competitive Co-IP experiments suggested that PHGDH promotes the association of SYK and dectin-1 and inhibits the association of SYK and SHP-1

Fig. 4 PHGDH is indispensable for anti-fungal immunity. A *Wt* and *Phgdh* $^{-/-}$ BMDMs were infected with *Af* or *C. albicans* for 12 h or stimulated or unstimulated zymosan, curdlan, zymd, α-mannan, flagellin, or malp-2 for 24 h. TNF-α and IL-6 levels in the supernatants were measured using ELISA ($n = 3$ mice per condition, two-way ANOVA, mean ± SEM). **B** *Wt* or *Phgdh* $^{-/-}$ were injected with *C. albicans* through the tail vein and monitored for survival; the Kaplan-Meier survival curve was plotted to determine the survival rate. Statistical analysis was performed using the log-rank test ($n = 5$ for each group). **C** *Wt* or *Phgdh* $^{-/-}$ were injected with *C. albicans* for 48 h. The kidney, spleen, and liver homogenates were plated on YPD media for 24 h; then, colonies were counted, and fungal burden was determined ($n = 3$ for each group). **D** Experiments were performed as described in **C**, except serum pro-inflammatory cytokines were measured using ELISA. **E** *Wt* or *Phgdh* $^{-/-}$ were infected with *C. albicans* for 3 d, and levels of IFN-γ and IL-17A in the supernatant of splenic cells were measured using ELISA ($n = 4$ for each group). **F** *Wt* or *Phgdh* $^{-/-}$ were infected with *C. albicans* for three days. Then, splenic cells were isolated, and intracellular staining of IFN-γ (Th1) and IL-17A (Th17) was determined using flow cytometry ($n = 4$ for each group). **G** Experiments, except serum IgG, were performed as described in **E** and measured using ELISA. **H** *Wt* and *Phgdh*$^{-/-}$ BMDMs were stimulated with zymd (100 μg/ml) and α-mannan (100 μg/ml) for the indicated times before Western blot. Experiments were repeated at least three times. Values in **C–G** are presented as means ± SEMs two-way ANOVA. (**$P < 0.01$). See also Fig. S4.

(Fig. 3H and 3I). Similar results were obtained via in vitro binding assays using purified proteins (Fig. S3G and S3H). Dectin or Mincle binds to ligands and attracts FcRγ, which serves as SYK's docking site. We next determined whether PHGDH would impact the interaction of SYK and FcRγ. As shown in Fig. 3J, PHGDH overexpression eliminated the inhibitory effect of SHP-1 on the dectin-1/SYK/FcRγ interaction. To examine the function of PHGDH in forming the dectin-1/SYK complex, we generated *Phgdh* knockout (*Phgdh* $^{-/-}$) mice and verified protein absence using Western blots (Fig. S3I). Zymd and α-mannan stimulation increased the interaction between SYK, dectin-1, and FcRγ in wild-type (WT) BMDMs but not *Phgdh* $^{-/-}$ BMDMs (Fig. 3K and 3L). We determined whether PHGDH promotes SYK recruitment to the cell membrane following stimulation. As shown in Fig. 3M, zymd and α-mannan stimulation induced SYK translocation to the membrane in *Wt* BMDMs but not *Phgdh*$^{-/-}$ BMDMs. These findings suggest that fungal infections promote the interaction of SYK and PHGDH, leading to SYK recruitment to the FcRγ.

PHGDH regulates anti-fungal innate immunity

Because PHGDH interacts with SYK and SYK is an essential protein in CLR signaling cascades, we suspected PHGDH regulates CLR signaling. As expected, TNF-α and IL-6 production was substantially lower in *Phgdh*$^{-/-}$ BMDMs than in control *Wt* BMDMs on stimulation with *Af*, *C. albicans*, zymosan, curdlan, zymd, and α-mannan, but not flagellin and malp-2 (Fig. 4A). To further characterize the in vitro function of PHGDH anti-fungal immune responses, we intravenously infected *Wt* mice and *Phgdh*$^{-/-}$ mice with a lethal dose of *C. albicans*. The *Phgdh*$^{-/-}$ mice showed less resistance to fungal infection than *Wt* mice (Fig. 4B). Consistently, *Phgdh*$^{-/-}$ mice exhibited more *C. albicans* colony-forming units (CFU) in the kidney, spleen, and liver compared with *Wt* mice (Fig. 4C). In this vein, *Phgdh*$^{-/-}$ mice showed reduced levels of IL-6, TNF-α, IL-1β, CXCL1, and CXCL2 than *Wt* mice in response to *C. albicans* infection (Fig. 4D). A previous study demonstrated the regulation of Th1 and Th17 responses during fungal infection [30]. Intriguingly, IFN-γand IL-17A were attenuated in the kidneys from *Phgdh*$^{-/-}$ mice compared to *Wt* mice (Fig. 4E). Additionally, the percentage of Th1 and Th17 cells in the spleen was lower in *Phgdh*$^{-/-}$ mice compared with *Wt* mice (Fig. 4F). Given that *C. albicans* is the primary inducer of anti-fungal immunoglobulin G (IgG), we observed that after five days of infection, *Phgdh*$^{-/-}$ mice produced significantly less serum IgG in comparison to *Wt* mice (Fig. 4G). Next, we tested whether PHGDH regulated SYK-mediated CLR pathways. Western blot analyses revealed that the phosphorylation of SYK in *Phgdh*$^{-/-}$ BMDMs was attenuated in response to zymd and α-mannan stimulation compared to that in *Wt* BMDMs (Fig. 4H). SYK-dependent phosphorylation of PLCγ2 and PKCδ, as well as phosphorylation of the downstream molecular ERK, JNK, p65, and p38, were also attenuated in *Phgdh*$^{-/-}$ BMDMs, compared with *Wt* BMDMs (Fig. 4H).

Previous studies have shown that the *C. albicans* yeast produces signals through dectin-1 by recognizing β-glucan, while the hyphal form makes signals through dectin-2 and -3 by identifying α-mannan [31]. As expected, *Phgdh*$^{-/-}$ BMDMs displayed a significant reduction in the production of pro-inflammatory factors compared with *Wt* BMDMs on infection with *C. albicans* hyphae or yeast (Fig. S4A and S4B). To determine whether PHGDH plays a similar role in response to other fungal species, we infected *Wt* mice and *Phgdh*$^{-/-}$ mice with *Af*; *Phgdh*$^{-/-}$ mice showed significantly greater mortality than *Wt* mice (Fig. S4C). *Phgdh*$^{-/}$mice consistently exhibited a more significant fungal burden in the lung at 48 h after infection than in control mice (Fig. S4D). We infected *Phgdh*$^{-/-}$ BMDMs and *Wt* BMDMs with various fungal morphotypes of *Af* and measured pro-inflammatory factor levels in the supernatants. As shown in Fig. S4E–S4H, *Phgdh*$^{-/-}$ BMDMs produced lower amounts of IL-6, TNF-α, IL-1β, CXCL1, and CXCL2 than in *Wt* BMDMs in response to dormant conidia, swollen conidia, or germ tube (GT) stimulation. These findings suggest that PHGDH positively regulates SYK-associated signaling cascades in the CLR pathway.

SYK regulates SSP, one-carbon metabolism, and redox homeostasis during fungal infection

Because PHGDH interacts with SYK, and PHGDH is the first rate-limiting enzyme of the SSP, we suspected that SYK regulates the SSP. To test this hypothesis, we created *Syk* knockout (*Syk* $^{-/-}$) mice and confirmed protein absence using Western blots (Fig. S5A). As expected, *Af*-infected BMDMs displayed higher ^{13}C-glucose incorporation into G6P, 3PG, lactate, serine, and glycine, but not PEP (Fig. 5A). However, *Af* infection did not affect lactate, serine, or glycine in *Syk*$^{-/-}$ BMDMs (Fig. 5A). Interesting, PHGDH-overexpressing BMDMs displayed higher ^{13}C-glucose incorporation into lactate, serine, and glycine, but not PEP (Fig. 5B). However, PHGDH overexpression did not affect ^{13}C-glucose incorporation in *Syk*$^{-/-}$ BMDMs (Fig. 5B). In agreement with previous results, a metabolomic analysis indicated that *C. albicans* treatment induced expression of G6P, 3PG, lactate, serine, and glycine but reduced PEP; *Syk* knockout removed the effect of *C. albicans* on glucose metabolism reprogramming (Fig. S5B). Previous studies demonstrated that the phosphorylation of PHGDH is essential to its activity and cellular location [32]. We found that *Af* infection enhanced PHGDH activity and PHGDH phosphorylation in *Wt* BMDMs but not in *Syk* $^{-/-}$ BMDMs (Fig. 5C). SYK overexpression induced PHGDH activity and PHGDH phosphorylation in a dose-dependent manner (Fig. 5D). Next, we used a kinase-dead mutant of Syk (Syk K402R) [33] to investigate if the increase in PHGDH activity in response to SYK overexpression is caused by SYK catalytic activity. As anticipated, SYK WT overexpression enhanced PHGDH activity; however, Syk K402R did not affect PHGDH activity (Fig. 5E). In vitro kinase assays showed that recombinant Syk (WT), but not Syk K402R, phosphorylate PHGDH

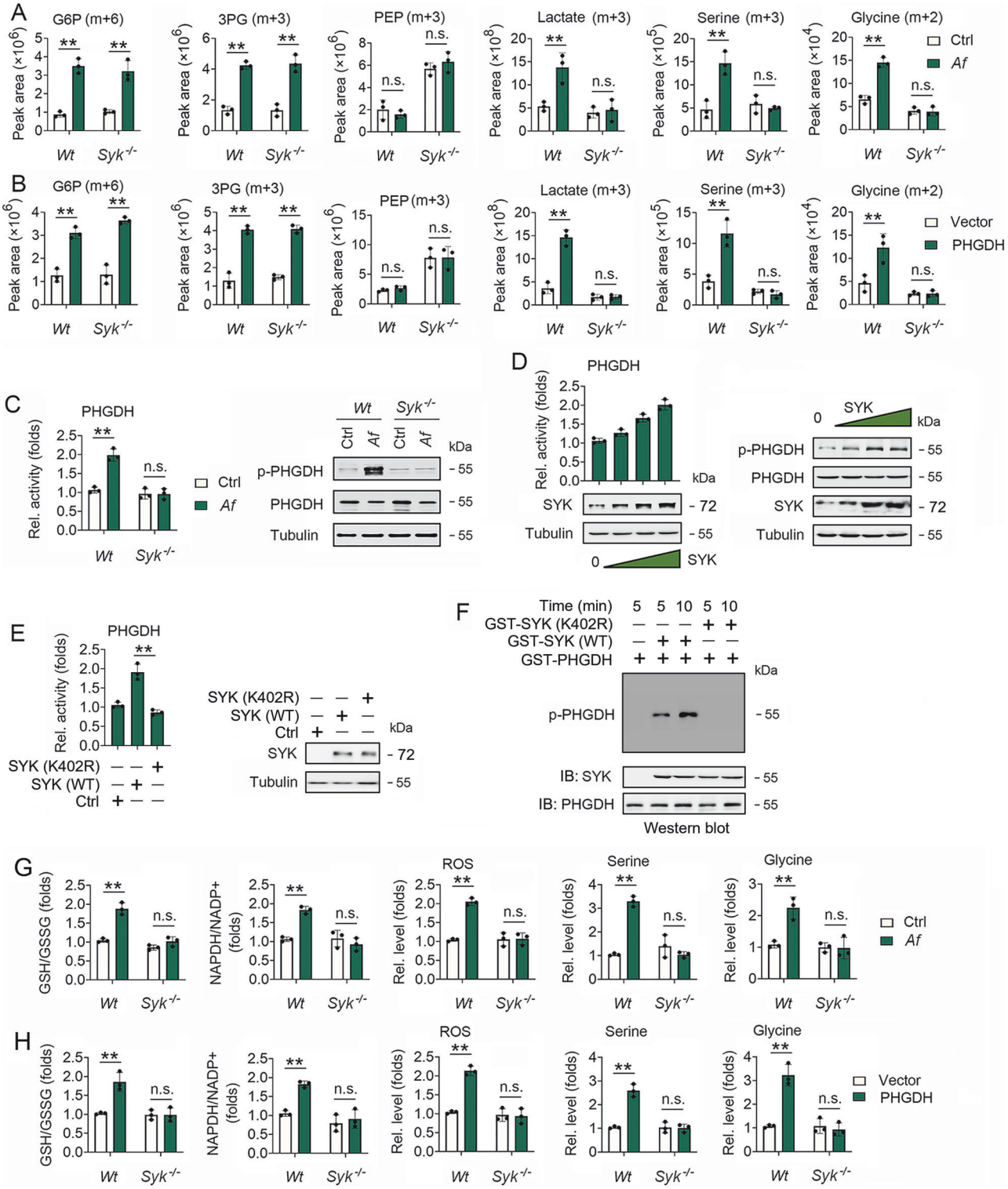

Fig. 5 SYK is indispensable for fungal-regulated metabolism. A *Wt* and *Syk* $^{-/-}$ BMDMs were infected with or without *Af* for 6 h. ^{13}C-glucose incorporation into G6P, 3PG, PEP, lactate, serine, and glycine was measured. **B** *Wt* and *Syk* $^{-/-}$ BMDMs were transfected with vector controls or pCMV-PHGDH for 36 h. ^{13}C-glucose incorporation into G6P, 3PG, PEP, lactate, serine, and glycine was analyzed. **C** *Wt* and *Syk* $^{-/-}$ BMDMs were infected with or without *Af* for 4 h, followed by an analysis of PHGDH activity (left panel) and PHGDH phosphorylation (right panel). **D** *Wt* BMDMs were transfected with increasing amounts of SYK expression plasmids for 4 h, followed by an analysis of PHGDH activity (left panel) and PHGDH phosphorylation (right panel). **E** *Syk* $^{-/-}$ BMDMs were transfected with indicated plasmids for four h, followed by an analysis of PHGDH activity. **F** GST-PHGDH, GST-SYK, and/or GST-SYK (K402R) were incubated in a kinase reaction buffer containing [γ-^{32}P]ATP for the indicated times, followed by autoradiography analyses (upper panel) or Western blot analyses (lower panel). **G** *Wt* and *Syk* $^{-/-}$ BMDMs were infected with or without *Af* for 6 h, followed by measurement of the GSH/GSSH ratio, the NADPH/NADP$^+$ ratio, ROS, serine, and glycine levels. **H** Experiments were performed as described in **E**, except *Wt* and *Syk* $^{-/-}$ BMDMs were transfected with PHGDH expression plasmids. Values in **A–F** are presented as means ± SEMs, $n = 3$ per condition, two-way ANOVA. (**$P < 0.01$, n.s., not significant). See also Fig. S5.

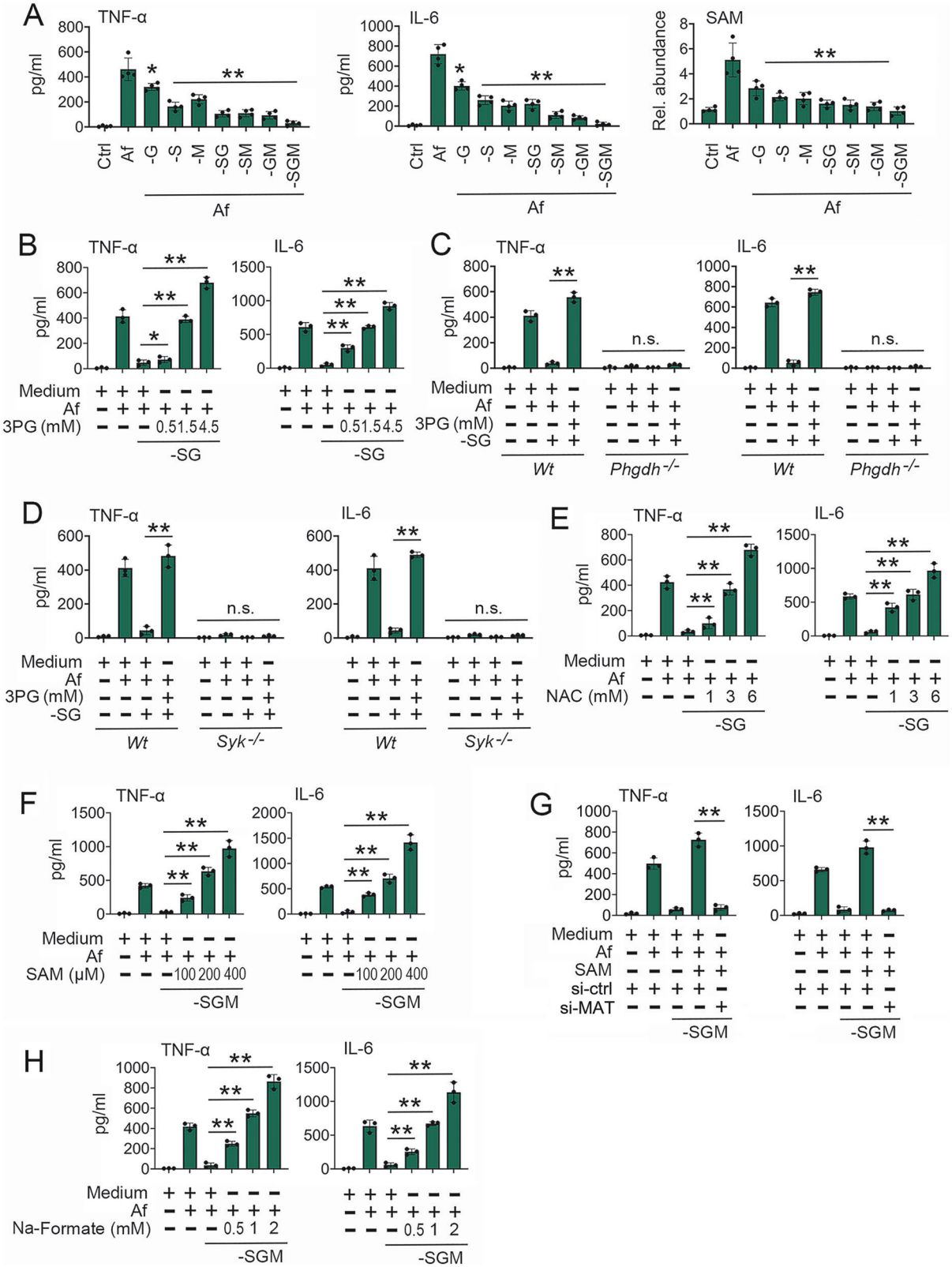

(Fig. 5F). Next, we sought to determine the role of SYK on the PPP pathway. As shown in Fig. 5G, *Af* infection enhanced the GSH/GSSG ratio, the NADPH/$NADP^+$ ratio, reactive oxygen species (ROS), serine, and glycine levels in *Wt* BMDMs but not *Syk* $^{-/-}$ BMDMs. Intriguingly, PHGDH overexpression also increased the GSH/GSSG ratio, the NADPH/$NADP^+$ ratio, and ROS, serine, and glycine levels in *Wt* BMDMs, while SYK depletion removed this effect (Fig. 5H). The role of SYK on the PPP pathway is not *Af*-specific because similar results were observed in *C. albicans*-infected BMDMs (Fig. S5C–S5H). These findings suggest that SYK is required for fungal infection-regulated PPP, the SSP, and redox homeostasis.

Fig. 6 Exogenous methionine and serine corporately support fungal-induced inflammation by fueling SAM generation. A BMDMs were starved for serine, glycine, and methionine for 12 h, after which the media were replaced with matched media deficient in the indicated amino acid (s) in the presence of *Af* for 6 h. Levels of TNF-α and IL-6 were measured using ELISA, and levels of SAM were measured using LC-MS. **B** Experiments were performed as described in **A**, except cells were treated with indicated concentrations of 3PG for 6 h. **C** *Wt* and *Phgdh* $^{-/-}$ BMDMs were starved for serine and glycine for 12 h, after which the media were replaced with matched media deficient of indicated amino acid (s). Then, cells were infected with or without *Af* or treated with or without 3PG (1.5 mM) for 6 h. TNF-α and IL-6 levels in the supernatant were measured using ELISA. **D** Experiments were performed as described in **C**, except *Wt* and *Syk* $^{-/-}$ BMDMs were used. Experiments were performed as described in **B**, except for the indicated concentrations of NAC **E** and SAM **F**, which were used. **G** BMDMs were transfected with indicated siRNA and starved for serine, glycine, and methionine for 12 h, after which the media were replaced with matched media deficient in the indicated amino acid (s) in the presence of Af for 6 h. Levels of TNF-α and IL-6 were measured using ELISA. **H** Experiments were performed as described in **B**, except for the indicated concentrations of formate used. Values in **A–H** are presented as means ± SEMs, $n = 3$ per condition, two-way ANOVA. (**$P < 0.01$, *$P < 0.05$, n.s., not significant). See also Fig. S6.

Exogenous methionine and serine support anti-fungal innate immunity by fueling SAM generation

In a medium with normal extracellular serine levels, PHGDH inhibition exhibits an anti-inflammatory phenotype, indicating that exogenous serine may not be a crucial function of the SSP in anti-fungal innate immunity. To test this hypothesis, we added various concentrations of exogenous serine; however, this did not affect NCT503 inhibited TNF-α and IL-6 production (Fig. S6A). The addition of the thiol reductant N-acetylcysteine (NAC), as well as threonine (Thr), glycine (Gly), methionine (Met), pyruvate (Pyr), homocysteine (Hcy), and α-ketoglutarate (α-KG), also did not affect this suppressed TNF-α or IL-6 production (Fig. S6B–S6H). Neither exogenous nor SSP-derived serine-derived one-carbon units could be used for homocysteine re-methylation to create methionine, and the SSP-derived serine constituted a tiny portion of the total serine pool. Therefore, we postulated that exogenous serine and methionine may enhance anti-fungal innate immunity as important donors of one-carbon units and methyl groups. Consistent with this hypothesis, depletion of serine (-S), methionine (-M), or their combined depletion (-SM), (-GM), and (-SM) resulted in the suppression of *Af*-induced TNF-α, IL-6, and SAM levels (Fig. 6A). In contrast, the depletion of glycine alone (-G) had a limited effect (Fig. 6A), possibly because low expression of glycine decarboxylase (GLDC) in BMDMs (Fig. S6I). One-carbon units and methyl groups restrict the deprivation of serine, glycine, and methionine (-SGM). As expected, -SGM almost eliminated *Af*-induced TNF-α, IL-6, and SAM levels (Fig. 6A). Similar results were obtained in zymd or α-mannan-treated BMDMs (Fig. S6J and S6K). 3PG channels into the SSP from glycolysis in the event of a serine deficiency. In contrast to the inability of exogenous serine to prevent the anti-inflammatory effect of SSP blockade, additional 3PG (1.5 mM and 4.5 mM) enhanced, 3PG (0.5 mM) mildly enhanced, IL-6 and TNF-α production under -SG conditions (Fig. 6B). Furthermore, SSP compensation did not affect IL-6 and TNF-α production in *Phgdh*$^{-/-}$ BMDMs or *Syk* $^{-/-}$ BMDMs (Fig. 6C and 6D). The addition of NAC and SAM was sufficient to fully restore the suppressed TNF-α and IL-6 production by -SGM (Fig. 6E and 6F). By contrast, MAT knockdown removes the effort of SAM on TNF-α and IL-6 production under -SGM conditions (Fig. 6G). The SSP synchronizes using one-carbon units in nucleotide synthesis by preventing the waste of one-carbon units [34]. Consistent with this finding, formate (which reacts directly with THF to make 10-formyl-THF) alleviated this anti-inflammatory effect of SSP blockade (Fig. 6H). Similarly, 3PG, NAC, formate, and SAM fully restored -SGM-inhibited TNF-α and IL-6 production in response to zymd or α-mannan stimulation (Fig. S6L and S6M). These findings suggest that exogenous serine and methionine play critical roles in anti-fungal innate immunity by fueling SAM generation.

SAM generation and its driven methylation reactions coordinately modulate histone methylation modifications during fungal infection

Histone H3 is susceptible to histone methylation. Trimethylation at lysines 4, 27, and 36 (H3K4me3, H3K27me3, and H3K36me3) is one of several methylation marks on histone H3 that significantly control gene expression [35]. SAM is the universal substrate for histone methylation[35]. Therefore, we speculated that a histone modification state would change during fungal infection. As shown in Fig. 7A–D, and S7A–S7C, *Af* infection substantially increased H3K36me3 levels, but mildly increased levels of H3K36me1, H3K36me2 and H3K27ac. 3DZA and PF9366 treatment removed *Af*-induced H3K36me3 expression, but not H3K36me1 and H3K36me2 expression (Figs. 7A, 7B and S7A). Consistent with 3DZA and PF9366 effects on SAM generation, -S, -M, -SG, -SM, -GM, and -SGM suppressed *Af*-induced H3K36me3, while other histone methylation marks were less affected (Figs. 7C and S7B). Additional 3PG, NAC, formate, and SAM fully restored -SGM-inhibited H3K36me3 expression, but not H3K36me1 and H3K36me2 expression (Figs. 7D and S7C). The RNA polymerase II elongation footprint marker H3K36me3 is elevated after TSSs in active genes and coincides with transcriptionally active regions [36]. We used chromatin immunoprecipitation combined with qPCR (ChIP-qPCR) to ascertain how Af infection affects the H3K36me3 chromatin occupancy of certain inflammatory genes. As shown in Figs. 7E and S7D, *Af* infection increased H3K36me3 binding to promoters of IL-6, TNF-α, IL-1β, and CXCL2, whereas NCT503, RZ-2994, PF9366, and 3DZA treatment decreased H3K36me3 binding to these gene promoters. Similar results were obtained by using si-PHGDH, si-SHMT2 and si-MAT (Fig. 7F). As expected, -S, -M, -SG, -SM, -GM, and -SGM each suppressed *Af*-induced H3K36me3 binding to promoters of IL-6, TNF-α, IL-1β, and CXCL2 (Figs. 7G and S7E). Additional 3PG, NAC, formate, and SAM fully restored -SG-inhibited H3K36me3 binding to these gene promoters (Figs. 7H and S7F). NSD1/2/3, ASH1L, SETD3, and SETMAR are enzymes that catalyze H3K36 mono or bi-methylation, while SETD2 is the only reported histone trimethylase catalyzing the trimethylation of H3K36 [37–39]. We next screen which enzymes play an important role in anti-fungal innate immunity. We designed two siRNAs for NSD1/2/3, ASH1L, SETD3, SETMAR, and SETD2, and tested their efficiency (Fig. S7G). As expected, H3K36me3 was greatly diminished in SETD2 knockdown cells (Fig. S7H). SETD2 knockdown inhibited *Af*, zymd or α-mannan-induced levels of IL-6, TNF-α, IL-1β, and CXCL2 (Fig. S7I–S7K). However, NSD1, ASH1L, SETD3, and SETMAR knockdown did not affect *Af*-regulated levels of IL-6 and TNF-α (Fig. S7L). These findings suggest that H3K36me3 is an epigenetic modification associated with Af infection.

The PHGDH/SYK axis regulates amino acid metabolism, and epigenetic modification predicts outcomes in patients infected with *Af* and *C. albicans*

We obtained fresh blood from healthy individuals (HI), acute invasive aspergillosis patients (AIAP), acute invasive candidiasis patients (AICP), convalescent aspergillosis patients (CAP), and convalescent candidiasis patients (CCP). There were two independent cohorts of fungal-infected patients. Cohort #1 included 56 HI, 40 AIAP, and 34 CAP. Cohort #2 included 40 HI, 37 AICP, and 35 CCP. To investigate whether PHGDH/SYK axis-regulated pathways

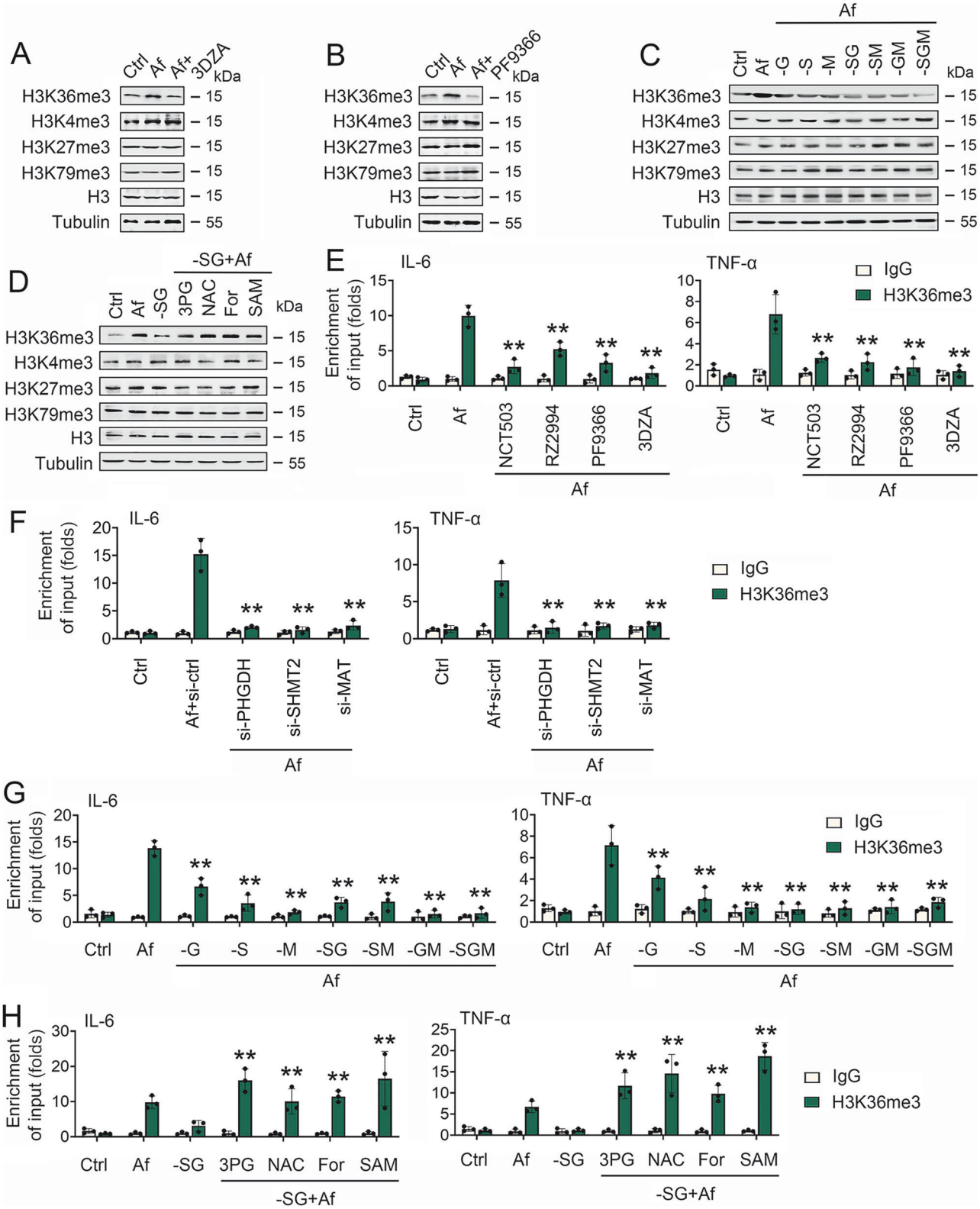

predicted outcomes in fungal-infected patients, we measured inflammatory cytokine expression and metabolites in the SSP, the PPP, and one-carbon metabolism in Cohort #1. IL-6, TNF-α, IL-1β, and CXCL2 were expressed at significantly higher levels in AIAP, whereas these inflammatory cytokines returned to normal in CAP (Fig. S8A). The activity of PHGDH and serine and glycine levels, the GSH/GSSG ratio, and the NADPH/$NADP^+$ ratio were significantly higher in AIAP. However, lower in CAP (Fig. 8A). Elevated PHGDH activity, serine, and glycine levels, the GSH/GSSG ratio, and the NADPH/$NADP^+$ ratio in AIAP tightly correlated with IL-6 and TNF-α expression (Fig. 8B and 8C). We randomly selected four HI, AIAP, and CAP. Co-IP experiments revealed that PHGDH was associated

Fig. 7 SAM generation and methylation reactions coordinately modulate histone methylation marks during fungal-induced inflammation. A BMDMs were infected with or without *Af* and treated with or without 3DZA (1 μM) for 6 h before Western blot analyses. **B** Experiments were performed as described in **A** except PF9366 (10 μM) was used. **C** BMDMs were starved for serine, glycine, and methionine for 12 h, after which the medium was replaced with a matched medium deficient in the indicated amino acid(s) in the presence of *Af* for 6 h before Western blot analyses. **D** Experiments were performed as described in **C**, except NAC (3 mM), formate (1 mM), and SAM (200 μM) were used. **E** BMDMs were infected with or without *Af* and treated with or without NCT503 (50 mM), RZ-2994 (10 μM), PF9366 (10 μM), or 3DZA (1 μM) for 6 h. ChIP assays were performed with anti-H3K36me3- or IgG-conjugated agarose. Gene sequences in the input DNA and the DNA recovered from antibody-bound chromatin segments were measured using qPCR. **F** BMDMs were transfected with indicated siRNAs for 24 h and infected with or without *Af* for 6 h before ChIP assays. **G** BMDMs were starved for serine, glycine, and methionine for 12 h, after which the media were replaced with matched medium deficient in the indicated amino acid(s) in the presence of *Af* for 6 h before ChIP assays. **H** Experiments were performed as described in **G**, except 3PG (1.5 mM), NAC (3 mM), formate (1 mM), and SAM (200 μM) were used. Experiments in **A–D** were repeated at least three times. Values in **E–H** are presented as means ± SEMs, $n = 3$ per condition, two-way ANOVA. (**$P < 0.01$, n.s., not significant). See also Fig. S7.

with SYK in PBMCs from AIAP. This association was dismissed in PBMCs from CAP (Fig. 8D). The phosphorylation of PHGDH and SYK and H3K36me3 levels were more significant in PBMCs from three randomly selected AIAPs. In contrast, the phosphorylation of PHGDH and SYK was inhibited in CAP (Fig. 8E and 8F). Further experiments indicated that H3K36me3 bound to promoters of IL-6, TNF-α, IL-1β, and CXCL2 in AIAP but not in CAP (Fig. 8G–I).

Subsequently, we analyzed inflammatory cytokine expression and metabolites in the SSP and the PPP in Cohort #2. Similarly, inflammatory cytokine expression, PHGDH activity, serine and glycine levels, the GSH/GSSG ratio, and the NADPH/$NADP^+$ ratio were significantly higher in AICP but lower in CCP (Fig. S8B and S8C). Elevated PHGDH activity, serine, and glycine levels, the GSH/GSSG ratio, and the NADPH/$NADP^+$ ratio in AICP were tightly correlated with IL-6 and TNF-α expression (Fig. S8D and S8E). Consistent with results in AIAP, H3K36me3 bound to promoters of IL-6, TNF-α, IL-1β, and CXCL2 in AICP but not in CCP (Fig. S8F–S8H). These findings suggest that one-carbon metabolism supports SAM and histone methylation, representing potential molecular markers for outcome prediction.

DISCUSSION

In this study, we discovered a hitherto unreported mechanism of fungal infection-induced reprogramming of glucose metabolism, whereby increased glycolysis offshoots are supported in the production of inflammatory factors. After looking into the processes underlying this occurrence, we discovered that fungal infection caused SYK associated with PHGDH, which activated the SSP, one-carbon metabolism, and CLR signaling. SAM is an essential metabolite that supports innate defense against fungi by epigenetically activating inflammatory genes. Our research uncovers a novel role for amino acid metabolism in CLR signaling and advances our understanding of anti-fungal innate immunity.

The energy source for cellular metabolism is glucose [18]. CLRs are crucial for host defense against fungal infections because they can identify different components of the fungal surface [40]. Many heritable variations in gene expression that do not result in changes to the gene sequence are referred to as “epigenetics” [41]. However, it is still unknown if the three systems communicate with one another when a fungal infection occurs. Here, we demonstrated for the first time that one-carbon flow, epigenetic alteration, and anti-fungal innate immunity are directly correlated (Fig. 9). We discovered that one-carbon metabolism has a synergistic effect on innate immunity against fungal infections by adjusting the availability of SAM to facilitate the epigenetic reprogramming of histone methylation (Fig. 9). An elevated SAM/SAH ratio is necessary for H3K36me3 to function as an epigenetic mark (Fig. 9). After looking into the processes underlying this occurrence, we discovered that the association between SYK and PHGDH is essential for all three systems (Fig. 9). But we also found that fungal infection caused a change in the glucose flux into the PPP; this phenomenon cannot be entirely explained by the PHGDH and SYK connection. When thinking about the next phase, studies delving into the mechanism might elucidate anti-fungal innate immunity. We also examined the order of one-carbon flux, epigenetic change, and innate defense against fungal infections. We discovered that the three systems do not act in parallel. Activated metabolites during a fungal infection could emerge in as little as an hour (Fig. S1). However, inflammatory factor production was found as early as three hours following fungal infection (Fig. S1). These results suggest that innate immunity against fungal infection is downstream of metabolism-regulated histone modification.

One-carbon metabolism has gained renewed attention due to identifying frequent tumor-specific changes in the expression of one-carbon metabolic enzymes [42]. For instance, serine metabolism plays a role in cancer cells’ fast growth by providing one-carbon units needed for nucleotide synthesis [43]. Nonetheless, immune cells often have a limited ability to proliferate [26]. This paradox led us to wonder about the physiological roles that one-carbon units made from serine play in anti-fungal innate immunity when combined with exogenous absorption and the SSP. We demonstrated that the SSP or exogenous serine-derived single carbons are infrequently employed as methyl groups for methylation processes through homocysteine re-methylation. As a result, during fungus infection, the methionine and folate cycles separate. Subsequent research revealed that exogenous serine and the PPP-derived ribose, one-carbon units supplied by the SSP, work in concert to enhance de novo ATP generation. The methionine cycle, which uses ATP as its primary methyl donor, produces SAM and inflammatory factors. Interestingly, ATP is an active metabolite and energy carrier essential for cell survival and proliferation. However, this work shows that ATP is a structural precursor of SAM needed for synthesizing inflammatory factors and nucleic acids. According to our research, immune cells do not grow as quickly as tumor cells but tend to create cytokines. Additional exogenous formate can restore the inflammatory factor expression of a blocked SSP, but additional exogenous serine cannot. These findings suggest that the SSP might be involved in more modulatory functions than just supplying one-carbon units; conversely, exogenous methionine might be the primary methyl donor for the synthesis of SAM and the expression of inflammatory factors. It is noteworthy that specific tumor cells have also shown the modulatory influence of the SSP on one-carbon flow efficiency.

To sum up, our research sheds light on how several nutritional inputs work together to feed the production of SAM during fungal infection. SAM activates innate immunity against fungi by regulating the chromatin state. Identifying H3K36me3 as a mediator between anti-fungal innate immunity and metabolism suggests a possible treatment strategy for invasive fungal infections.

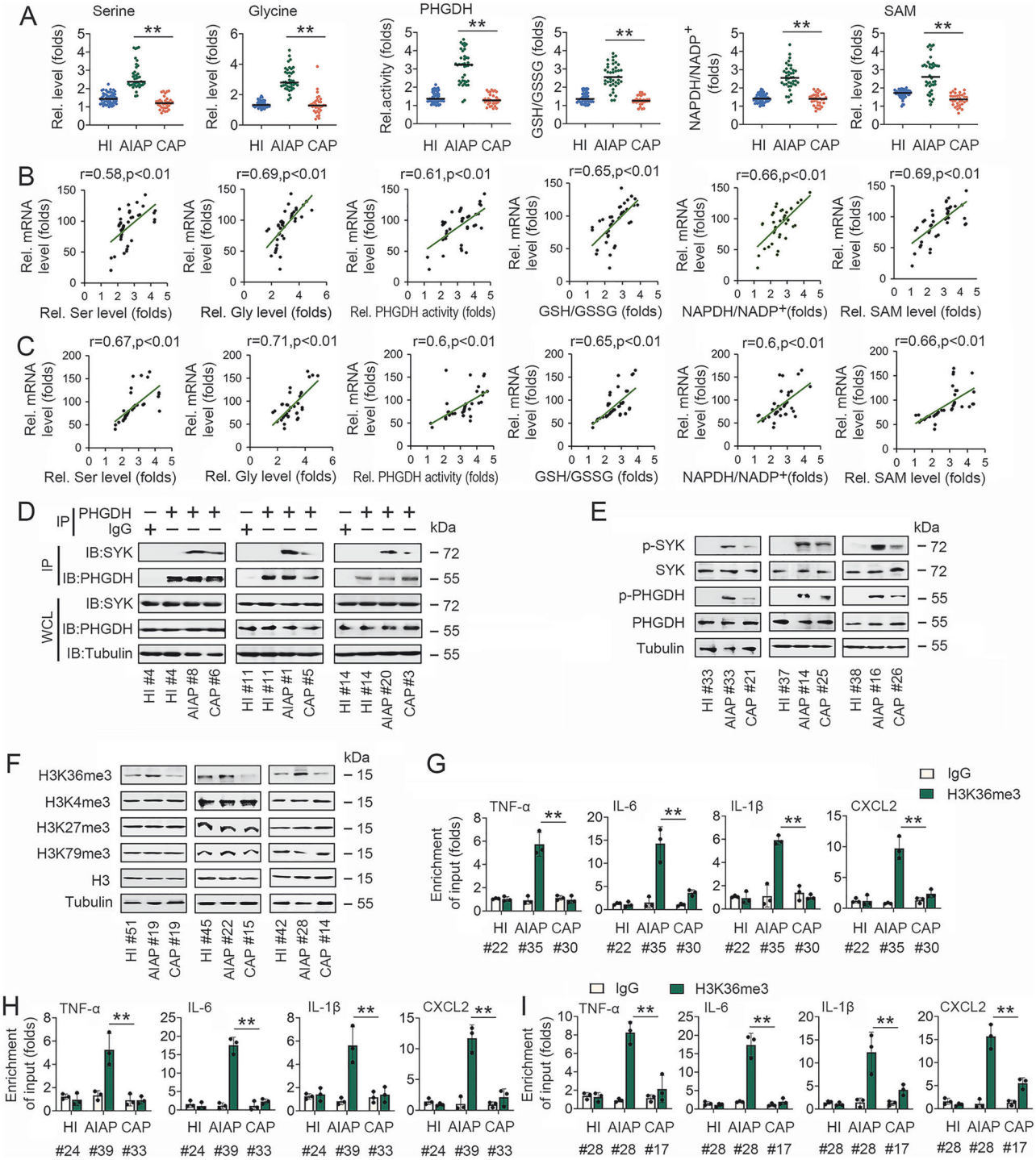

Fig. 8 Immunometabolites in the PPP, the SSP, and one-carbon metabolism correlate with inflammatory factor expression in fungal-infected patients. A Serine, glycine, and SAM levels, PHGDH activity, GSH/GSSG, and NADPH/NADP$^+$ ratios in PBMCs of healthy individuals (HI) ($n = 56$), acute invasive aspergillosis patients (AIAP) ($n = 40$), and convalescent aspergillosis patients (CAP) ($n = 34$). The lowest value of HI was designated as 1. All Values are expressed as fold-induction (fold) relative to the lowest value of HI. Values represent means ± SEM. **B** TNF-α mRNA levels and serine, glycine, SAM levels, PHGDH activity, GSH/GSSG, and NADPH/NADP$^+$ ratios in PBMCs of AIAP subjected to Pearson's correlation analysis. **C** IL-6 mRNA levels and serine, glycine, SAM levels, PHGDH activity, GSH/GSSG, and NADPH/NADP$^+$ ratios in PBMCs of AIAP subjected to Pearson's correlation analysis. **D** PBMCs were isolated from indicated HI, AIAP, and CAP. Co-IP and immunoblot analyses were performed with the indicated antibodies. **E, F** PBMCs were isolated from indicated HI, AIAP, and CAP. Immunoblot analyses were performed with the indicated antibodies. **G–I** PBMCs were isolated from indicated HI, AIAP, and CAP. ChIP assays were performed with anti-H3K36me3- or IgG-conjugated agarose. TNF-α, IL-6, IL-1β, and CXCL2 sequences in the input DNA, and the DNA recovered from antibody-bound chromatin segments was measured using qPCR. Values represent means ± SEM. (**$P < 0.01$). See also Fig. S8.

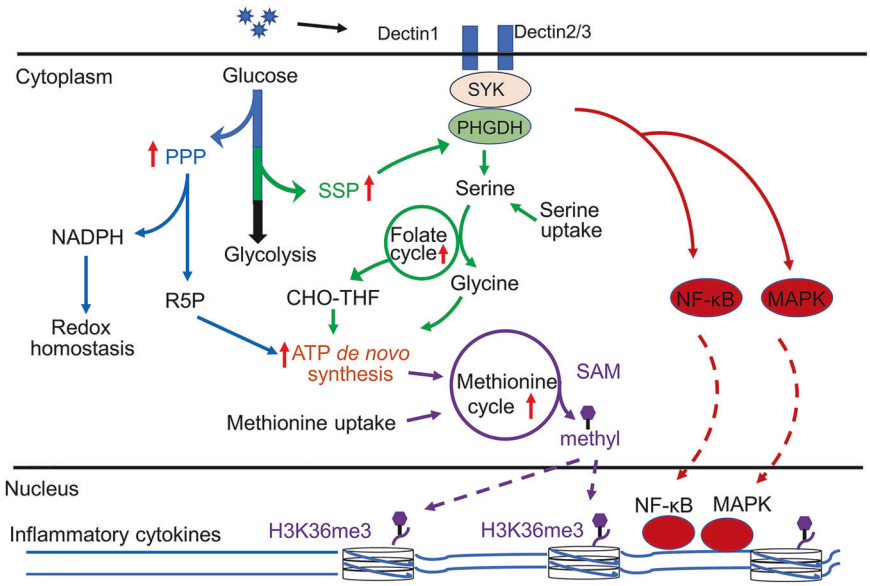

Fig. 9 The synergistic effects of the PPP, the SSP, the folate cycle, and the methionine cycle on SAM generation and inflammatory regulation in the context of fungal infection. During fungal infection, SYK binds to PHGDH, leading to the activation of PHGDH. Then, metabolic flux drives a switch from glycolysis to the SSP, folate, and methionine cycles for SAM generation. As a result, epigenetic reprogramming and pro-inflammatory cytokines and chemokines are produced. PHGDH associates with SYK, enabling SYK to bind to CLRs. As a result, SYK-associated signaling cascade activation results in pro-inflammatory cytokine and chemokine production. (Blue, green, and purple arrows indicate the metabolic flux of the PPP, the SSP, and the methionine cycle, respectively. The red arrow indicates the SYK-associated signaling cascades).

DATA AVAILABILITY

The original contributions presented in the study are included in the article or the supplementary material. This paper does not report original code. Other data that support the findings are available from the corresponding author upon reasonable request.

REFERENCES

1. Brown GD, Denning DW, Gow NA, Levitz SM, Netea MG, White TC. Hidden killers: human fungal infections. Sci Transl Med. 2012;4:165rv113.
2. Fisher MC, Hawkins NJ, Sanglard D, Gurr SJ. Worldwide emergence of resistance to antifungal drugs challenges human health and food security. Science. 2018;360:739–42.
3. Arastehfar A, Carvalho A, Houbraken J, Lombardi L, Garcia-Rubio R, Jenks JD, et al. Aspergillus fumigatus and aspergillosis: From basics to clinics. Stud Mycol. 2021;100:100–15.
4. Morrell M, Fraser VJ, Kollef MH. Delaying the empiric treatment of candida bloodstream infection until positive blood culture results are obtained: a potential risk factor for hospital mortality. Antimicrob Agents Chemother. 2005;49:3640–5.
5. Sanglard D. Emerging threats in antifungal-resistant fungal pathogens. Front Med. 2016;3:11.
6. Romani L. Immunity to fungal infections. Nat Rev Immunol. 2011;11:275–88.
7. Hardison SE, Brown GD. C-type lectin receptors orchestrate antifungal immunity. Nat Immunol. 2012;13:817–22.
8. Mocsai A, Ruland J, Tybulewicz VL. The SYK tyrosine kinase: a crucial player in diverse biological functions. Nat Rev Immunol. 2010;10:387–402.
9. Gross O, Gewies A, Finger K, Schäfer M, Sparwasser T, Peschel C, et al. Card9 controls a non-TLR signalling pathway for innate anti-fungal immunity. Nature. 2006;442:651–6.
10. Geijtenbeek TB, Gringhuis SI. Signalling through C-type lectin receptors: shaping immune responses. Nat Rev Immunol. 2009;9:465–79.
11. Cueto FJ, Del Fresno C, Sancho D. DNGR-1, a dendritic cell-specific sensor of tissue damage that dually modulates immunity and inflammation. Front Immunol. 2019;10:3146.
12. Chabner BA, Roberts TG. Jr. Timeline: Chemotherapy and the war on cancer. Nat Rev Cancer. 2005;5:65–72.
13. Ducker GS, Rabinowitz JD. One-carbon metabolism in health and disease. Cell Metab. 2017;25:27–42.
14. Kory N, Wyant GA, Prakash G, UitdeBos J, Bottanelli F, Pacold ME, et al. SFXN1 is a mitochondrial serine transporter required for one-carbon metabolism. Science. 2018;362:eaat9528.
15. Shyh-Chang N, Locasale JW, Lyssiotis CA, Zheng Y, Teo RY, Ratanasirintrawoot S, et al. Influence of threonine metabolism on S-adenosylmethionine and histone methylation. Science. 2013;339:222–6.
16. Locasale JW. Serine, glycine and one-carbon units: cancer metabolism in full circle. Nat Rev Cancer. 2013;13:572–83.
17. Ma EH, Bantug G, Griss T, Condotta S, Johnson RM, Samborska B, et al. Serine is an essential metabolite for effector T cell expansion. Cell Metab. 2017;25:482.
18. DeBerardinis RJ, Thompson CB. Cellular metabolism and disease: what do metabolic outliers teach us? Cell. 2012;148:1132–44.
19. Liu X, Cooper DE, Cluntun AA, Warmoes MO, Zhao S, Reid MA, et al. Acetate production from glucose and coupling to mitochondrial metabolism in mammals. Cell. 2018;175:502–513 e513.
20. Lewis CA, Parker SJ, Fiske BP, McCloskey D, Gui DY, Green CR, et al. Tracing compartmentalized NADPH metabolism in the cytosol and mitochondria of mammalian cells. Mol Cell. 2014;55:253–63.
21. Li X, Sun X, Carmeliet P. Hallmarks of endothelial cell metabolism in health and disease. Cell Metab. 2019;30:414–33.
22. Lee WD, Pirona AC, Sarvin B, Stern A, Nevo-Dinur K, Besser E, et al. Tumor reliance on cytosolic versus mitochondrial one-carbon flux depends on folate availability. Cell Metab. 2021;33:190–8 e196.
23. Ashkavand Z, O'Flanagan C, Hennig M, Du X, Hursting SD, Krupenko SA. Metabolic reprogramming by folate restriction leads to a less aggressive cancer phenotype. Mol Cancer Res. 2017;15:189–200.
24. Nilsson R, Jain M, Madhusudhan N, Sheppard NG, Strittmatter L, Kampf C, et al. Metabolic enzyme expression highlights a key role for MTHFD2 and the mitochondrial folate pathway in cancer. Nat Commun. 2014;5:3128.
25. Gonçalves SM, Duarte-Oliveira C, Campos CF, Aimanianda V, Ter Horst R, Leite L, et al. Phagosomal removal of fungal melanin reprograms macrophage metabolism to promote antifungal immunity. Nat Commun. 2020;11:2282.
26. Yu W, Wang Z, Zhang K, Chi Z, Xu T, Jiang D, et al. One-carbon metabolism supports s-adenosylmethionine and histone methylation to drive inflammatory macrophages. Mol Cell. 2019;75:1147–60.
27. Pikman Y, Ocasio-Martinez N, Alexe G, Dimitrov B, Kitara S, Diehl FF, et al. Targeting serine hydroxymethyltransferases 1 and 2 for T-cell acute lymphoblastic leukemia therapy. Leukemia. 2022;36:348–60.
28. Sedding DG, Tröbs M, Reich F, Walker G, Fink L, Haberbosch W, et al. 3-deazaadenosine prevents smooth muscle cell proliferation and neointima formation by interfering with ras signaling. Circulation Research. 2009;104:1192–1200.
29. Nguyen TA, Pang KC, Masters SL. Intercellular communication for innate immunity. Mol Immunol. 2017;86:16–22.

30. Richardson JP, Moyes DL. Adaptive immune responses to Candida albicans infection. Virulence. 2015;6:327–37.
31. Zhu LL, Zhao XQ, Jiang C, You Y, Chen XP, Jiang YY, et al. C-type lectin receptors Dectin-3 and Dectin-2 form a heterodimeric pattern-recognition receptor for host defense against fungal infection. Immunity. 2013;39:324–34.
32. Ma C, Zheng K, Jiang K, Zhao Q, Sha N, Wang W, et al. The alternative activity of nuclear PHGDH contributes to tumour growth under nutrient stress. Nat Metab. 2021;3:1357–71.
33. Coopman PJP, Do MTH, Barth M, Bowden ET, Hayes AJ, Basyuk E, et al. The Syk tyrosine kinase suppresses malignant growth of human breast cancer cells. Nature. 2000;406:742–7.
34. Reid MA, Allen AE, Liu S, Liberti MV, Liu P, Liu X, et al. Serine synthesis through PHGDH coordinates nucleotide levels by maintaining central carbon metabolism. Nat Commun. 2018;9:442.
35. Henikoff S, Shilatifard A. Histone modification: cause or cog? Trends Genet. 2011;27:389–96.
36. Shilatifard A. Chromatin modifications by methylation and ubiquitination: implications in the regulation of gene expression. Annu Rev Biochem. 2006;75:243–69.
37. Topchu I, Pangeni RP, Bychkov I, Miller SA, Izumchenko E, Yu J, et al. The role of NSD1, NSD2, and NSD3 histone methyltransferases in solid tumors. Cell Mol Life Sci. 2022;79:285.
38. Lam UTF, Tan BKY, Poh JJX, Chen ES. Structural and functional specificity of H3K36 methylation. Epigenetics & Chromatin. 2022;15:17.
39. Chen K, Liu J, Liu S, Xia M, Zhang X, Han D, et al. Methyltransferase SETD2-mediated methylation of STAT1 Is critical for interferon antiviral activity. Cell. 2017;170:492–506.
40. Wang X, Zhang H, Shao Z, Zhuang W, Sui C, Liu F, et al. TRIM31 facilitates K27-linked polyubiquitination of SYK to regulate antifungal immunity. Signal Transduct Target Ther. 2021;6:298.
41. Liu S, Liu L, Xu G, Cao Z, Wang Q, Li S, et al. Epigenetic modification is regulated by the interaction of influenza a virus nonstructural protein 1 with the De Novo DNA methyltransferase DNMT3B and subsequent transport to the cytoplasm for K48-linked polyubiquitination. J Virol. 2019;93:e01587-18.
42. Locasale JW, Grassian AR, Melman T, Lyssiotis CA, Mattaini KR, Bass AJ, et al. Phosphoglycerate dehydrogenase diverts glycolytic flux and contributes to oncogenesis. Nat Genet. 2011;43:869–74.
43. Possemato R, Marks KM, Shaul YD, Pacold ME, Kim D, Birsoy K, et al. Functional genomics reveal that the serine synthesis pathway is essential in breast cancer. Nature. 2011;476:346–50.

AUTHOR CONTRIBUTIONS

QWW and ADC conceived and designed the experiment. XYY, DDH, XYS,YCG and YZ performed the experiments.CXS, SL,CYZ and GPL analyzed the data. XYY, DDH and ADC processed and typeset the figures. SL, CYZ and QWW wrote the manuscript. All authors read and approved the final manuscript.

FUNDING

This work was supported by the National Key Research and Development Program of China (2021YFC2701800, 2021YFC2701804), the Fundamental Research Funds for the Central Universities (2042022dx0003), the Fundamental Research Funds for the Central Universities (2042021kf023), the National Natural Science Foundation of China (81872262) and Deutsche Forschungsgemeinschaft (Transregio TRR60).

COMPETING INTERESTS

The authors have declared that no conflict of interest exists.

ETHICS

The guidelines outlined in the Declaration of Helsinki were followed when collecting clinical samples. The Nanjing Medical University Institutional Review Board authorized protocols that adhered to standards for the safety of human participants. Each study participant gave written informed consent for sample collection and analysis. Mice were raised and used in particular pathogen-free environments following Nanjing Medical University-approved guidelines. The National Institutes of Health Guide for the Care and Use of Laboratory Animals was followed in all animal experimentation.

ADDITIONAL INFORMATION

Supplementary information The online version contains supplementary material available at https://doi.org/10.1038/s41418-024-01374-7.

Correspondence and requests for materials should be addressed to Qiwen Wu or Aidong Chen.